THE ASTROPHYSICAL JOURNAL, 402:623–634, 1993 January 10

MASS LOSS FROM PRE–MAIN-SEQUENCE ACCRETION DISKS. I. THE ACCELERATING WIND OF FU ORIONIS

NURIA CALVET[1]
Centro de Investigaciones de Astronomia, Ap. P. 264 Mérida 5101-A, Venezuela
AND
LEE HARTMANN[2] AND SCOTT J. KENYON[2]
Harvard-Smithsonian Center for Astrophysics, 60 Garden Street, Cambridge, MA 02138
Received 1992 February 6; accepted 1992 July 20

ABSTRACT

We present evidence that the wind of the pre–main-sequence object FU Orionis arises from the surface of the luminous accretion disk. A disk wind model calculated assuming radiative equilibrium explains the differential behavior of the observed asymmetric absorption-line profiles. The model predicts that strong lines should be asymmetric and blueshifted, while weak lines should be symmetric and double-peaked due to disk rotation, in agreement with observations. We propose that many blueshifted "shell" absorption features are not produced in a true shell of material, but rather form in a differentially expanding wind that is rapidly rotating. The inference of rapid rotation supports the proposal that pre–main-sequence disk winds are rotationally driven. FU Ori may lose substantial amounts of mass over a significant area of the innermost disk ($\sim$10 stellar radii), which could have important implications for the structure of jets from young stellar objects. Our results support the suggestion that massive winds originate from rapidly accreting pre–main-sequence accretion disks.

Subject headings: accretion, accretion disks — stars: mass loss — stars: pre–main-sequence

1. INTRODUCTION

The discovery of powerful bipolar outflows from pre–main-sequence objects indicates that mass loss plays an important role in star formation (Lada 1985; Shu, Lizano, & Adams 1987; Edwards, Ray, & Mundt 1992 and references therein). Bipolar outflows appear to be quite common in the earliest stages of star formation (Terebey, Vogel, & Myers 1989) and can easily disperse the material surrounding the central source. In certain cases, long and remarkably thin optical "jets" of material emanate from young objects (Reipurth 1989). The kinetic energy carried by these jets often amounts to $\gtrsim 10\%$ of the total system luminosity (Lada 1985).

The most popular theories for producing bipolar flows or jets from young stars tap the energy liberated as material accretes through a circumstellar disk onto the central star (Adams, Lada, & Shu 1987; Kenyon & Hartmann 1987; Bertout, Basri, & Bouvier 1988; Basri & Bertout 1989). In these theories, high-velocity gas is ejected either from a rapidly rotating central star (Hartmann & MacGregor 1982; Shu et al. 1988; Ruden, Glassgold, & Shu 1990) or from an accretion disk (Pudritz & Norman 1983; Königl 1989; Pringle 1989; Pelletier & Pudritz 1992). In both types of models, material is flung outward along strong magnetic field lines anchored in the star or in the disk (Fig. 1). The rotating magnetic field ultimately collimates the flow into bipolar jets (e.g., Blandford & Payne 1982).

The source of the mass loss from young stars is controversial, because many bipolar flow sources are heavily reddened and therefore not directly observable. However, optical observations can be employed to study the wind acceleration region in several young FU Orionis variables that have powerful outflows and are not strongly reddened (Reipurth 1989, 1990; Hartmann, Kenyon, & Hartigan 1991). FU Orionis objects are thought to be pre–main-sequence disks undergoing rapid mass accretion at rates of $\dot{M}_{\rm acc} \gtrsim 10^{-4}\ M_\odot\ {\rm yr}^{-1}$ (Hartmann & Kenyon 1985; Hartmann et al. 1992) and thus provide good laboratories for studying the connection between pre–main-sequence disk accretion and mass loss. The prototype of the class, FU Ori, has a strong wind with a terminal wind velocity $v \sim 300$ km s^{-1} detected in the strong Hα line and a mass-loss rate $\sim 10^{-5}\ M_\odot\ {\rm yr}^{-1}$ (Herbig 1966; Bastian & Mundt 1985; Crosswell, Hartmann, & Avrett 1987).

If FU Ori has a disk wind, spectral lines of different strengths should display different profiles. Strong lines, formed in the outermost disk atmosphere, should exhibit strongly blueshifted absorption components. Conversely, weak lines formed in deeper, denser disk layers should exhibit profiles in which rotation dominates, since by mass conservation the expansion velocities will be small in dense regions (Fig. 1). The line profiles should vary continuously as the line opacity increases, so that lines of intermediate strength should exhibit intermediate (small) blueshifts. Observations provide qualitative support for this picture; strong Fe II lines exhibit "shell" absorption at velocities of ~ -80 to -50 km s^{-1} (Herbig 1966; Petrov & Herbig 1992), while weak lines are symmetric and double-peaked. In addition, moderately strong photospheric lines in the blue spectral region are asymmetric and show blueshifts of ~ -10 km s^{-1} (Hartmann & Kenyon 1985, 1987a, b; Kenyon, Hartmann, & Hewett 1988, hereafter KHH; Welty et al. 1992). Although this behavior is consistent with a disk wind, no quantitative model for the lines has yet been constructed.

To test the disk wind hypothesis by comparing with observed line profiles, it is necessary to construct wind models which account for the variable ionization and line excitation as

[1] Also Grup d'Astrofisica de la Societat Catalana de Fisica, Institut d'Estudis Catalans.

[2] Visiting Astronomer, Kitt Peak National Observatory, operated by the National Optical Astronomy Observatory under contract to the National Science Foundation.

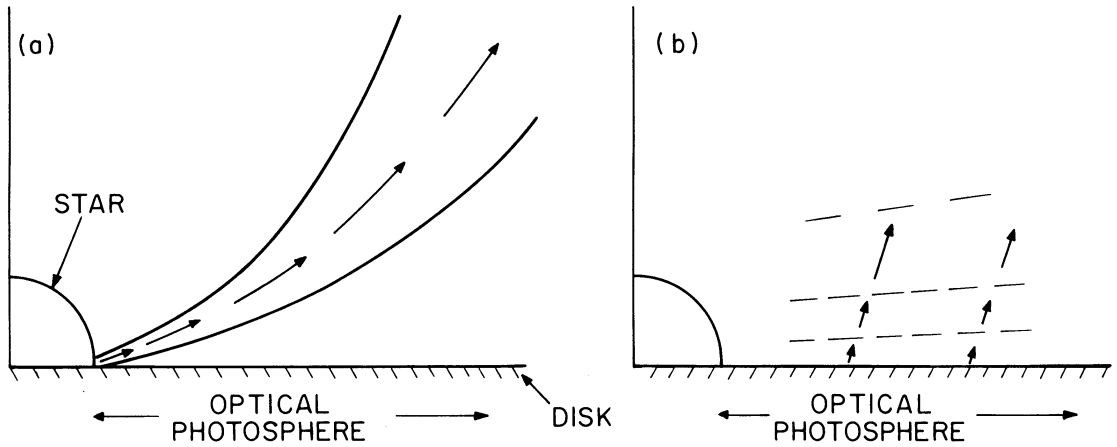

FIG. 1.—Schematic depiction of two types of rotationally driven, magnetically accelerated winds from pre–main-sequence objects. (*a*) Disk accretion spins up a central star, causing mass to be ejected from near the rapidly rotating stellar equator. (*b*) A wind emanates from the pre–main-sequence accretion disk, in which the vertical velocity increases with increasing distance from the disk.

a function of height above the disk and radial distance from the central star. In this paper we present model atmosphere calculations for a pre–main-sequence accretion disk with a massive wind. We treat the accelerating regions near the disk surface, and so assume plane-parallel geometry. For our initial investigation we adopt a schematic velocity structure for the disk wind, calculate the wind temperature assuming radiative equilibrium, and compute line profiles assuming LTE populations for the neutral and singly ionized metals. The models quantitatively agree with observed profiles of a few specific lines in FU Ori with greatly differing strengths and explain some general trends in profile shapes and asymmetries found by Petrov & Herbig (1992).

In addition, we suggest that many sharp blueshifted "shell" absorption features in FU Ori are not formed in a shell of roughly constant velocity, but rather arise in a rapidly expanding, *rotating* wind. The suggestion of rapid rotation supports the theories of disk wind acceleration by rotating magnetic field lines advanced by Blandford & Payne (1982), Pudritz & Norman (1983), and Königl (1989).

2. CALCULATIONS

2.1. *Disk Atmosphere*

We consider a viscous, geometrically thin, optically thick accretion disk with constant mass accretion rate $\dot{M}_{\rm acc}$ surrounding a star with mass M and radius R_i. The reference height H measured in the direction outward from the disk midplane (z) varies with cylindrical radius r as $H = H_0(r/R_i)^{9/8}$. We take $H_0 = 0.1R_i$, which is consistent with some theoretical models of FU Ori objects (Clarke, Lin, & Pringle 1990). Our results are not sensitive to the choice of disk thickness; the photospheric lines are sensitive only to order of magnitude changes in the surface gravity, which is proportional to H.

Our radiative transfer solutions assume that spectral lines form close to the (geometrically thin) disk, so we neglect radial energy transport and adopt a plane-parallel geometry. We first calculate a plane-parallel model atmosphere at each disk annulus assuming hydrostatic equilibrium, as discussed in detail by Calvet et al. (1991b). This model neglects viscous dissipation within the photosphere (see Hartmann & Kenyon 1991 for a justification), so radiative equilibrium holds and viscous energy generation in deeper disk layers determines the surface radiative flux. The constant radiative flux through the optically thick disk atmosphere can be characterized by an effective temperature

$$T_{\rm eff} = \left\{\frac{3GM\dot{M}_{\rm acc}}{4\pi\sigma r^3}\left[1 - \left(\frac{R_i}{r}\right)^{1/2}\right]\right\}^{1/4} \quad (1)$$

(Shakura & Sunyaev 1973; Lynden-Bell & Pringle 1974). The vertical temperature structure is calculated using the gray atmosphere approximation in the Eddington approximation for a Rosseland mean optical depth τ. To calculate the structure of the atmosphere at each radius r we assume that the reference height H corresponds to the level $\tau = 2/3$, and solve by iteration the system of equations

$$\frac{dp}{d\tau} = \frac{g(z)}{\chi_{\rm Ross}}, \quad (2)$$

$$\frac{dz}{d\tau} = -\frac{1}{\chi_{\rm Ross}\rho}, \quad (3)$$

where the height-dependent gravity is given by

$$g(z) = \frac{GM(H + z)}{[r^2 + (z + H)^2]^{3/2}}. \quad (4)$$

Here $\chi_{\rm Ross}$ is the Rosseland mean opacity, ρ is the density, and z is the height of the atmosphere above $\tau = 2/3$. Atomic and molecular populations are calculated assuming LTE.

Having initially calculated a radiative equilibrium atmosphere assuming hydrostatic equilibrium throughout, we then modify the structure by introducing a schematic disk wind. For simplicity we assume that material flows away from the disk midplane in the vertical (z) direction at a velocity v. We further assume that the mass loss per unit area ρv at cylindrical disk radius r varies as

$$(\rho v)_r = (\rho v)_0\left(\frac{r}{R_i}\right)^{-a_1} = \frac{\dot{M}_0}{4\pi R_i^2}\left(\frac{r}{R_i}\right)^{-a_1}, \quad (5)$$

where $\dot{M}_0$ and a_1 are constant input parameters. In practice, we set $a_1 = 2$ to correspond to the self-similar disk wind solutions of Blandford & Payne (1982) (see § 2.3).

We need to join the wind to the disk atmosphere to compute line profiles of weak and intermediate-strength lines. Well above the disk photosphere, we adopt a velocity law $v(r, z)$ and

compute the density from mass conservation for steady flow. In the dense disk regions, we expect the material to be in vertical hydrostatic equilibrium. Typical wind models show density distributions which depart from hydrostatic equilibrium only when the flow velocity becomes comparable to or greater than the sound (or slow-mode) velocity (e.g., Hartmann & MacGregor 1982). We therefore adopt the simple expedient of using the hydrostatic atmosphere below a critical level z_s, and a wind velocity structure above z_s. At each r we define z_s from the relation

$$(\rho v)_r(z_s) = \rho_s c_s , \quad (6)$$

where ρ_s is the density given by the hydrostatic equilibrium solution and c_s is the adiabatic sound speed ($\gamma = 5/3$). We assume that the flow smoothly accelerates outward; therefore the flow is subsonic for $z < z_s$ and supersonic for $z > z_s$.

The line profiles are not very sensitive to the velocity at which the two solutions are joined. Any line with a noticeable velocity shift must be formed in a region where the wind velocity is a significant fraction of the rotational velocity. Since FU Ori rotates at ~ 65 km s^{-1} in the optical spectral region, many times the sound speed ~ 5 km s^{-1}, lines with significant wind-produced asymmetries must be formed in regions where the flow is highly supersonic, and thus well above z_s.

The velocity structure of a rotating hydromagnetic wind depends in detail on several parameters including the magnetic field strength and structure that are not currently predictable from first principles (Blandford & Payne 1982; Lovelace, Wang, & Sulkanen 1987). The flow velocities of the spherically self-similar models of Blandford & Payne (1982) scale as $V(z/r) \propto V_{\rm Kep}(r_0)$, where $V_{\rm Kep}$ is the Keplerian velocity where the field line enters the disk at $r = r_0$. The standard solution shown by Blandford & Payne indicates an expansion velocity that increases nearly linearly with height near the disk (their Fig. 4). We therefore adopt a simple parameterization of the vertical velocity structure and assume that the wind velocity increases linearly with distance above z_s:

$$v(r, z) = \Gamma V_{\rm Kep}(r)(z - z_s)/r + c_s(z_s) , \quad z_{\rm max} > z > z_s . \quad (7)$$

The density in the supersonic region is then given by

$$\rho(r, z) = \frac{(\rho v)_r}{v} , \quad (8)$$

with v determined by equation (7), and $z_{\rm max}$ is an arbitrary cutoff chosen so that $v(z_{\rm max}) = 100$ km s^{-1}.

With fixed $\rho(z)$, the new Rosseland optical depth and temperature scales are determined at each z by integrating inward from $z_{\rm max}$,

$$\tau(z) = \tau(z - \Delta z) + \chi[\rho(z), T(z)]\Delta z . \quad (9)$$

Using the gray Eddington expression for the temperature,

$$T(\tau)^4 = \tfrac{3}{4} T_{\rm eff}^4[\tau(z) + \tfrac{2}{3}] , \quad (10)$$

equation (9) can be solved as an implicit equation for $\tau(z)$. Finally, the pressure is calculated from the equation of state, interpolating at given density and temperature in precalculated tables of mean molecular weight.

The introduction of the wind, with finite continuum optical depth, increases the total optical depth in the subsonic region and thus increases the temperature for $z < z_s$. Consequently, the hydrostatic equilibrium solution for this region is no longer strictly self-consistent; but for most cases of interest, the change in the temperature is unimportant (see § 3.1). Similarly, the change in the optical depth scale due to addition of the wind also changes the effective gravity of the photosphere, since $g(z)$ is height-dependent, but our results are only sensitive to order-of-magnitude changes in gravity.

2.2. *Rotational Line Broadening*

Because our treatment is limited to regions near the disk photosphere, we assume that the outflowing material rotates at the same rate as the disk. The spectrum of an annulus at r, $I(r, \mu\Delta v)$, as a function of $\Delta v = (\lambda - \lambda_0)/c$ is calculated by convolving the appropriate rotational broadening function Ψ with the calculated nonrotationally broadened spectrum $I_{nr}(r, \mu, \Delta v)$,

$$I(r, \mu, \Delta v) = \int_{-\infty}^{+\infty} I_{nr}(r, \mu\Delta v')\Psi(\Delta v - \Delta v')d\,\Delta v' , \quad (11)$$

where $\mu = \cos i$, and

$$\Psi(\Delta v - \Delta v') = \{1 - [(\Delta v - \Delta v')/V_{\rm max}]^2\}^{-1/2}/\pi . \quad (12)$$

The parameter $V_{\rm max} = V_{\rm Kep}(r) \sin i$ is the projected rotational velocity of the annulus observed at inclination i. The line profile Ψ exhibits the well-known "double-peaked" shape of a rotating ring. The contributions of the different annuli are added together to produce the final spectrum for comparison with observations.

2.3. *Adopted Parameters*

To study the acceleration of the wind from photospheric levels outward, it is necessary to adopt a photospheric model, with an effective temperature, surface gravity, and projected rotational velocity of the disk as a function of radius. The central stellar mass, inner disk radius, accretion rate, and system inclination determine the photospheric properties and are constrained by observations of the disk luminosity, maximum disk temperature, and $v \sin i$ without reference to wind parameters. We adopt the accretion disk parameters used in our treatment of the near-infrared spectrum of FU Ori (Calvet, Hartmann, & Kenyon 1991a): $M = 0.49\ M_\odot$, $R_i = 4.42\ R_\odot$, $\dot{M}_{\rm acc} = 1.59 \times 10^{-4}\ M_\odot$ yr^{-1}, except that we take $i = 35°$ rather than $i = 40°$ to provide a slightly better match to the observed rotational velocities.

In the region of interest for our optical spectral synthesis ($R \lesssim 3R_i \lesssim 0.06$ AU), for a typical viscosity parameter $\alpha = 10^{-2}$ (Hartmann et al. 1992), we estimate a disk mass of $\lesssim 10^{-3}\ M_\odot$. Thus disk gravity is unimportant for the optical spectrum. At a typical radius of formation for the 2 μm CO spectrum, $R \sim 12R_i \sim 0.25$ AU, the disk mass would be $\sim 10^{-2}\ M_\odot$ for the same viscosity parameter, so the effects of self-gravity are not likely to be important either.

The final spectra were computed using a spectral-line list kindly provided by R. Kurucz. The *gf*-values were adjusted to provide agreement between the spectrum of a G supergiant and a nonrotating model atmosphere of appropriate effective temperature and gravity. (We used a G supergiant to provide the best match to the average optical spectrum of FU Ori; see KHH.)

In the context of the present simple model, the wind properties are fixed by the parameters $\dot{M}_0$, a_1, and Γ. The mass-loss parameter $\dot{M}_0$ is constrained by the results of Crosswell et al. (1987), who estimated a total mass-loss rate for the wind $\dot{M}_w \sim 10^{-5}\ M_\odot$ yr^{-1} for FU Ori from modeling the Hα and

Na I resonance lines. In our final models we adopt $\dot{M}_0 \sim 1 \times 10^{-5}\ M_\odot\ \mathrm{yr}^{-1}$. The other two wind parameters are not as well constrained by other considerations. We adopt $a_1 = 2$, as suggested by the self-similar wind solutions of Blandford & Payne (1982; possible departures from this behavior are discussed in § 3). For this choice, the total mass-loss rate from the disk at radii interior to r is

$$\dot{M}_w(r) = \dot{M}_0[\ln(r/R_i)] \ . \quad (13)$$

Finally, Γ was adjusted to produce the best agreement with observations. We found that $\Gamma = 1$ results in acceptable line profiles and is roughly consistent with the velocity law in the standard model of Blandford & Payne (1982).

The wind temperatures of the radiative equilibrium models are in reasonable agreement with the results of Crosswell et al. (1987), who estimated $T_w \sim 6000$ K for FU Ori; for comparison, at $r = 2R_i$, T_w asymptotically approaches 5420 K. At large distances above the disk, where gas densities are low, there may be departures from radiative equilibrium caused by adiabatic expansion and possible chromospheric heating. We ignore these effects for our initial exploration.

3. RESULTS

3.1. *Atmospheric Structure*

Tables 1–3 provide the detailed disk atmosphere structure at three radii of interest for the standard wind parameters. In Figure 2 we show the wind velocity versus optical depth (right panels) and the optical depth versus height for the initial static (without wind) models and the results with the wind (left panels).

TABLE 1

DISK ATMOSPHER STRUCTURE, $r = 1.36R_i$

z (cm)	ρ (g cm^{-3})	v (km s^{-1})	τ	T (K)
3.18E+11	2.84E−11	1.00E+02	3.49E−05	6.04E+03
3.01E+11	2.98E−11	9.50E+01	4.06E−03	6.05E+03
2.87E+11	3.12E−11	9.09E+01	8.01E−03	6.06E+03
2.67E+11	3.34E−11	8.49E+01	1.38E−02	6.07E+03
2.52E+11	3.52E−11	8.05E+01	1.81E−02	6.08E+03
2.37E+11	3.73E−11	7.61E+01	2.72E−02	6.10E+03
2.24E+11	3.93E−11	7.21E+01	3.57E−02	6.12E+03
2.07E+11	4.23E−11	6.69E+01	4.68E−02	6.15E+03
1.84E+11	4.71E−11	6.01E+01	6.14E−02	6.18E+03
1.70E+11	5.06E−11	5.60E+01	7.04E−02	6.20E+03
1.54E+11	5.53E−11	5.12E+01	8.06E−02	6.22E+03
1.36E+11	6.19E−11	4.58E+01	9.24E−02	6.24E+03
1.17E+11	7.03E−11	4.03E+01	1.06E−01	6.27E+03
9.74E+10	8.25E−11	3.43E+01	1.39E−01	6.34E+03
7.96E+10	9.77E−11	2.90E+01	1.82E−01	6.42E+03
6.36E+10	1.17E−10	2.42E+01	2.39E−01	6.52E+03
5.17E+10	1.37E−10	2.07E+01	3.14E−01	6.66E+03
4.12E+10	1.61E−10	1.76E+01	4.12E−01	6.82E+03
3.94E+10	1.66E−10	1.70E+01	5.40E−01	7.01E+03
3.87E+10	1.68E−10	1.68E+01	7.09E−01	7.24E+03
3.79E+10	1.71E−10	1.66E+01	9.30E−01	7.52E+03
3.68E+10	1.74E−10	1.62E+01	1.22E+00	7.84E+03
3.53E+10	1.79E−10	1.58E+01	1.60E+00	8.21E+03
3.34E+10	1.86E−10	1.52E+01	2.10E+00	8.63E+03
3.09E+10	1.96E−10	1.45E+01	2.76E+00	9.10E+03
2.76E+10	2.10E−10	1.35E+01	3.62E+00	9.62E+03
2.33E+10	2.32E−10	1.22E+01	4.75E+00	1.02E+04
1.76E+10	2.69E−10	1.05E+01	6.23E+00	1.08E+04
1.08E+10	3.35E−10	8.47E+00	8.18E+00	1.15E+04
9.23E+09	3.86E−10	7.34E+00	1.07E+01	1.23E+04

TABLE 2

DISK ATMOSPHERE STRUCTURE, $r = 2R_i$

z (cm)	ρ (g cm^{-3})	v (km s^{-1})	τ	T (K)
5.91E+11	1.31E−11	1.00E+02	6.40E−06	5.42E+03
5.64E+11	1.37E−11	9.53E+01	6.74E−04	5.42E+03
5.32E+11	1.45E−11	9.01E+01	1.53E−03	5.42E+03
5.04E+11	1.54E−11	8.54E+01	2.31E−03	5.42E+03
4.78E+11	1.62E−11	8.10E+01	3.04E−03	5.42E+03
4.52E+11	1.71E−11	7.67E+01	4.00E−03	5.43E+03
4.24E+11	1.82E−11	7.20E+01	5.25E−03	5.43E+03
3.87E+11	1.99E−11	6.57E+01	6.91E−03	5.43E+03
3.38E+11	2.28E−11	5.75E+01	9.09E−03	5.44E+03
3.08E+11	2.50E−11	5.25E+01	1.04E−02	5.44E+03
2.73E+11	2.80E−11	4.67E+01	1.20E−02	5.44E+03
2.36E+11	3.23E−11	4.06E+01	1.37E−02	5.45E+03
2.16E+11	3.53E−11	3.72E+01	1.57E−02	5.45E+03
1.92E+11	3.94E−11	3.32E+01	1.80E−02	5.45E+03
1.65E+11	4.56E−11	2.87E+01	2.07E−02	5.46E+03
1.34E+11	5.56E−11	2.36E+01	2.37E−02	5.47E+03
1.08E+11	6.84E−11	1.92E+01	3.12E−02	5.48E+03
7.54E+10	9.56E−11	1.37E+01	4.10E−02	5.50E+03
5.54E+10	1.26E−10	1.04E+01	4.70E−02	5.51E+03
3.92E+10	1.85E−10	7.13E+00	5.39E−02	5.52E+03
2.95E+10	3.53E−10	3.74E+00	7.09E−02	5.56E+03
1.51E+10	8.08E−10	1.63E+00	1.61E−01	5.72E+03
8.87E+09	1.09E−09	1.20E+00	2.79E−01	5.91E+03
6.37E+09	1.22E−09	1.07E+00	3.67E−01	6.05E+03
4.34E+09	1.33E−09	9.87E−01	4.82E−01	6.21E+03
2.64E+09	1.42E−09	9.24E−01	6.34E−01	6.40E+03
1.30E+09	1.49E−09	8.82E−01	8.34E−01	6.63E+03
2.93E+08	1.53E−09	8.59E−01	1.10E+00	6.91E+03
−4.21E+08	1.54E−09	8.50E−01	1.44E+00	7.22E+03
−9.40E+08	1.55E−09	8.46E−01	1.90E+00	7.57E+03
−1.33E+09	1.55E−09	8.45E−01	2.49E+00	7.99E+03
−1.40E+09	1.55E−09	8.45E−01	2.86E+00	8.17E+03
−1.53E+09	1.55E−09	8.45E−01	3.76E+00	8.59E+03
−1.60E+09	1.55E−09	8.46E−01	4.31E+00	8.84E+03
−1.86E+09	1.55E−09	8.46E−01	6.50E+00	9.77E+03
−1.95E+09	1.55E−09	8.48E−01	8.55E+00	1.02E+04
−2.08E+09	1.54E−09	8.49E−01	1.12E+01	1.08E+04

For $\dot{M}_0 = 10^{-5}\ M_\odot\ \mathrm{yr}^{-1}$, $a_1 = 2$, and $\Gamma = 1$, the optical depth of the wind modifies the temperature structure of the hydrostatic region very slightly at $R \gtrsim 2R_i$ (Fig. 2). At the innermost disk radius we take to have a wind, $r = 1.36R_i$, the density structure of the hydrostatic region is no longer self-consistent with the final temperature structure, but this does not affect the spectrum greatly because the photosphere is now formed in the wind. Because the continuum opacity depends strongly on temperature, the increase in $T_{\rm eff}$ from 6440 K at $2R_i$ to 7190 K at $1.36R_i$ causes the photosphere, $z(\tau \sim 2/3)$, to move to higher vertical distances, where the expansion velocity exceeds 10 km s^{-1}. Thus, *all photospheric lines* formed at $1.36R_i$ will be appreciably blueshifted.

Roughly 60% of the optical spectrum arises from disk annuli between 1.5 and $3R_i$ (KHH), which can be represented adequately by our results for $r = 2R_i$. The vertical structure at this annular distance begins to depart considerably from the purely static atmosphere when $\tau_{\rm Ross} \lesssim 2 \times 10^{-2}$ (Fig. 2). The wind velocity, $\gtrsim 30$ km s^{-1}, is already a significant fraction of the disk's projected rotational velocity of ~ 60 km s^{-1}, so lines formed at or above this level will exhibit profiles strongly affected by expansion.

The gaseous continuum opacity decreases rapidly with decreasing temperature, so the wind modifies the photospheric structure very slightly at $r = 8R_i$. We assume that dust formation occurs approximately for $T \leq 1500$ K, and this assump-

TABLE 3

DISK ATMOSPHERE STRUCTURE, $r = 8R_i$

z (cm)	ρ (g cm^{-3})	v (km s^{-1})	τ	T (K)
4.93E+12	8.19E−13	1.00E+02	6.05E−09	2.34E+03
4.47E+12	9.06E−13	9.04E+01	1.18E−06	2.34E+03
3.88E+12	1.05E−12	7.81E+01	2.91E−06	2.34E+03
3.21E+12	1.28E−12	6.40E+01	6.29E−06	2.34E+03
2.62E+12	1.58E−12	5.17E+01	9.25E−06	2.34E+03
2.29E+12	1.83E−12	4.48E+01	1.20E−05	2.34E+03
2.13E+12	1.97E−12	4.16E+01	1.36E−05	2.34E+03
1.80E+12	2.37E−12	3.45E+01	1.76E−05	2.34E+03
1.52E+12	2.85E−12	2.88E+01	2.28E−05	2.34E+03
1.29E+12	3.43E−12	2.39E+01	2.94E−05	2.34E+03
1.07E+12	4.23E−12	1.94E+01	3.81E−05	2.34E+03
8.69E+11	5.41E−12	1.51E+01	4.92E−05	2.34E+03
6.84E+11	7.26E−12	1.13E+01	7.24E−05	2.34E+03
4.63E+11	1.23E−11	6.65E+00	1.38E−04	2.34E+03
3.39E+11	3.92E−11	2.10E+00	4.38E−04	2.34E+03
2.96E+11	8.01E−11	1.03E+00	1.40E−03	2.34E+03
2.47E+11	1.82E−10	4.55E−01	5.74E−03	2.34E+03
2.29E+11	2.47E−10	3.35E−01	9.61E−03	2.34E+03
1.91E+11	4.52E−10	1.82E−01	2.69E−02	2.36E+03
1.70E+11	6.18E−10	1.33E−01	4.50E−02	2.37E+03
1.47E+11	8.45E−10	9.71E−02	7.52E−02	2.40E+03
9.87E+10	1.49E−09	5.54E−02	1.85E−01	2.48E+03
8.22E+10	1.74E−09	4.72E−02	2.39E−01	2.52E+03
6.43E+10	2.04E−09	4.02E−02	3.10E−01	2.57E+03
4.49E+10	2.38E−09	3.45E−02	4.00E−01	2.63E+03
2.28E+10	2.74E−09	2.99E−02	5.18E−01	2.70E+03
−3.42E+09	3.13E−09	2.62E−02	6.70E−01	2.78E+03
−3.70E+10	3.68E−09	2.23E−02	8.66E−01	2.88E+03
−7.92E+10	4.41E−09	1.86E−02	1.12E+00	2.99E+03
−1.32E+11	5.19E−09	1.58E−02	1.45E+00	3.12E+03
−2.17E+11	6.04E−09	1.36E−02	2.13E+00	3.34E+03
−2.92E+11	6.04E−09	1.36E−02	3.13E+00	3.61E+03
−3.57E+11	5.67E−09	1.44E−02	4.61E+00	3.92E+03
−4.24E+11	5.29E−09	1.55E−02	6.78E+00	4.27E+03
−4.80E+11	5.05E−09	1.62E−02	8.77E+00	4.52E+03
−5.13E+11	4.92E−09	1.66E−02	9.98E+00	4.67E+03

tion increases the wind continuum opacity dramatically for $r > 12R_i$. With $\dot{M}_0 = 10^{-5}\ M_\odot\ \mathrm{yr}^{-1}$ and $a_1 = 2$, the wind has $A_V \gtrsim 10^2$ at $r > 12R_i$ (assuming dust extinction similar to that of the interstellar medium). This is not permitted by the observations, because such a dusty wind would produce an enormous infrared excess that is not observed in FU Ori (Adams et al. 1987). The wind would also obscure the inner disk for a wide range of inclinations. We therefore assume that no mass loss occurs for disk radii $r > 12R_i$; however, we note that the formation and destruction of dust grains in the disk is quite uncertain. The issue of dust formation principally affects the calculation of the first-overtone CO lines, and we return to this point in §§ 3.5 and 4.

3.2. *Effects of Mass Loss on Optical Line Profiles*

To illustrate the effects of the wind, we consider three spectral lines which have qualitatively different behavior. The Li I 6707 Å line is always double-peaked in spectra of FU Ori (Hartmann et al 1991; Petrov & Herbig 1992; Welty et al. 1992). The strong Fe I 4957 Å line is generally not doubled, but roughly parabolic in shape, with little or no velocity shift (cf. Petrov & Herbig 1992; Welty et al. 1992). The Fe II 5018 Å line shows appreciable blueshifted absorption in a "shell" feature. We wish to explore whether a wind with a reasonable mass-loss rate can explain the differences in behavior among these lines.

We begin by examining the effects of differing mass-loss rates on the spectrum of a single annulus at $r = 3R_i$. The top row of panels in Figure 3 shows the height in the atmosphere where $\tau_\lambda = 1$ for the individual lines as a function of the velocity shift from line center. The Li I line always forms close to the photosphere for this range of mass-loss rates, and so it will not be affected by the wind. The Fe I line forms further away from the disk midplane than Li I, and so can be affected by the wind expansion if the mass-loss rate is sufficiently large. The Fe II 5018 Å line is formed still farther out in the atmosphere than the Fe I 4957 Å line, because Fe II is the dominant stage of ionization in the atmosphere, and thus is even more affected by the wind.

The middle row of panels shows the calculated line profiles at an inclination $i = 0°$, where there is no line broadening from rotation. The effect of the wind varies dramatically among the three lines considered. With high mass-loss rates, the strongest lines become blueshifted and broadened by expansion. The bottoms of the strong line profiles tend to be flat, which results from the assumption of plane-parallel geometry and LTE; the boundary temperature approaches a constant, and therefore the line source function is nearly constant in the outermost layers.

The bottom row of panels shows results for $i = 35°$, which provides the rotational broadening appropriate for FU Ori. With no mass loss, all three line profiles are double-peaked due to the Keplerian rotation of the annulus. As the wind increases in strength, the stronger lines become more asymmetric and blueshifted. At $\dot{M}_0 = 10^{-5}\ M_\odot\ \mathrm{yr}^{-1}$, the Fe II line shows no hint of double-peaked structure, but instead shows a strong, sharp, blueshifted "shell" absorption component. The Fe I line becomes asymmetric with slight doubling at this mass-loss rate, while the Li I line is formed so deeply in the atmosphere that it is unaffected by the wind and remains symmetric and double-peaked.

Perhaps the most surprising feature of Figure 3 is the development of a relatively sharp absorption "dip" in the Fe II line at $\dot{M}_0 = 10^{-5}\ M_\odot\ \mathrm{yr}^{-1}$, $i = 35°$. Comparing results for $i = 0°$ and $i = 35°$, one observes that this absorption "dip" or "shell" is not a true feature in the velocity structure of the wind, but arises from a combination of *rotation* and expansion. To demonstrate this more clearly, we present convolutions of schematic line profiles with the disk rotational broadening function in Figure 4. The left column of panels shows that convolution of a square profile with disk rotational broadening profile results in a profile with a pronounced central peak, as long as the rotational velocity and expansion velocity are comparable. In contrast, convolution of a triangular profile with the rotational broadening function does not produce such a significant peak (right row of panels in Fig. 4). Inspection of the wind model at $i = 0°$ in Figure 3 shows that the Fe II line satisfies these criteria for producing an absorption dip. As shown in the far-right panel of the middle row, the intrinsic line profile is fairly rectangular, and for $\dot{M}_0 = 10^{-5}\ M_\odot\ \mathrm{yr}^{-1}$, the width of the Fe II line is comparable to the rotational broadening velocity.

3.3. *Comparison with Optical Observations*

The emergent spectrum is the sum of spectra calculated for different annuli with differing rotational velocities and wind velocities. Figure 5 compares the resultant line profiles with observations of FU Ori obtained with the KPNO 4 m echelle spectrograph and TI CCD in December of 1988. Further

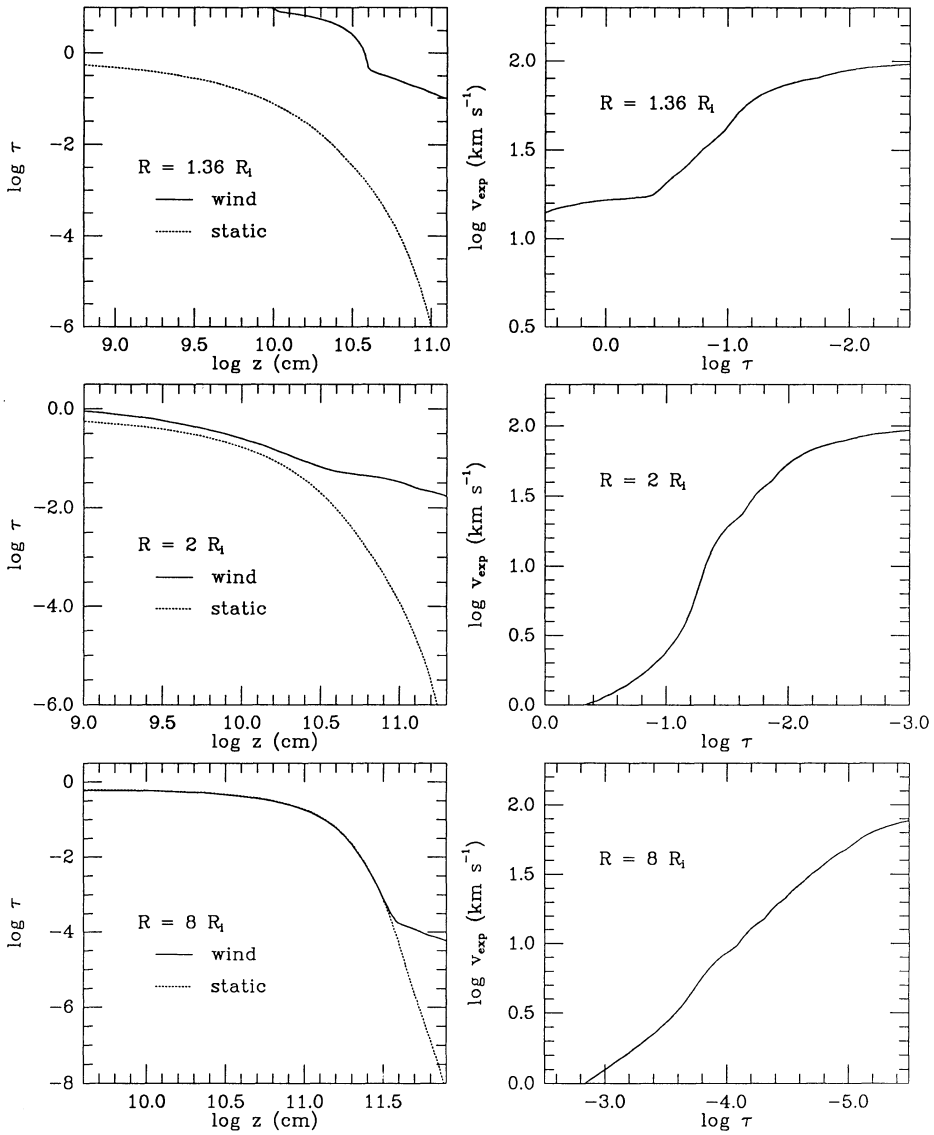

FIG. 2.—Vertical disk structure at three cylindrical radii. The left-most panels show the Rosseland mean optical scale vs. height for both the hydrostatic model (*dotted lines*) and the wind model (*solid lines*). The effect of the wind is to increase the optical depth at a given height. The right-most panels show the expansion velocity as a function of the optical depth scale. At the innermost radius considered, $r = 1.36R_i$, the *photosphere* is expanding at more than 10 km s^{-1}. At larger disk radii, only the optically thin layers are expanding significantly.

details of the observations and data reduction can be found in Hartmann & Stauffer (1989) and Hartigan et al. (1989).

The model predicts that the Li I line in FU Ori should be double-peaked, as observed, because it forms in a deep layer where the dominant motion is Keplerian rotation. We increased the Li abundance to log $N_{\rm Li} = 3.6$ (on a scale where log $N_{\rm H} = 12$), a factor of 2 or more increase over typical pre–main-sequence abundance estimates, to provide a better match with observations. The calculated equivalent width is still too small, but the Li I line is very temperature sensitive, and a modest change in the disk effective temperature might substantially improve the agreement with observation. In addition, non-LTE effects can increase the apparent abundance of Li in K supergiants by a factor of 2 (Steenbock & Holweger 1984), and such effects may be appropriate for the low-gravity photosphere of FU Ori.

The Fe II λ 5018 line lies in the blue spectral region, where line blending is extremely important. The effect of the wind is clearly demonstrated by comparison with the model with no mass loss. The wind model exhibits an absorption "dip," as observed. In our model, this absorption dip is not the result of a "shell" of material at nearly constant velocity (e.g., Herbig 1966), but instead arises from the convolution of rotation with the wind line profile, as described in the previous section.

We note that agreement between theory and observation requires strong Fe II absorption extending to blueshifts of $v_{\rm max} = 100$ km s^{-1}. At this velocity, with $\Gamma = 1$, $z \sim r$, the assumption of plane-parallel geometry breaks down. However, our model clearly predicts that the Fe II line must be very asymmetric, as observed.

The results for the Fe I 4957 Å "line" are complicated to interpret because this feature is actually a blend of several lines. Two strong Fe I lines from the same multiplet are present; the 4957.60 Å line dominates the blend, but the 4957.30 Å line

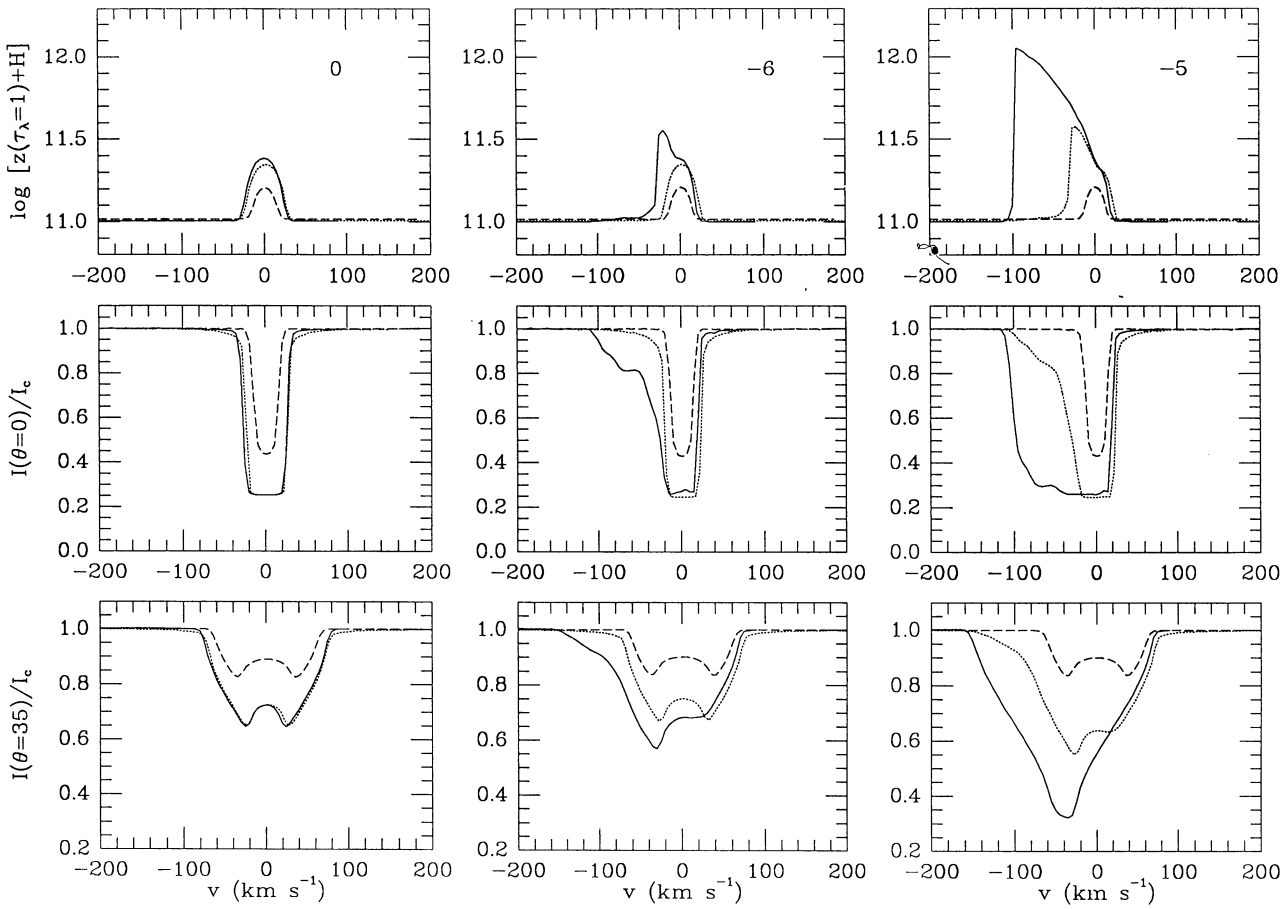

FIG. 3.—Line profile results for a disk annulus at $r = 3R_i$, for the Li I 6707 Å line (*dashed lines*), the Fe I 4957 Å line (*dotted lines*), and the Fe II 5018 Å (*solid lines*). The uppermost row of panels shows the heights at which $\tau_\lambda = 1$ is reached for each line at each velocity shift. The middle row of panels shows the line profiles observed at an inclination $i = 0°$, i.e., for no rotational broadening. The bottom panels show the resulting line profiles for $i = 35°$. The left-most vertical column shows results for no mass loss, and the other two columns exhibit results for $\dot{M}_0 = 10^{-6}\ M_\odot\ \mathrm{yr}^{-1}$ and $\dot{M}_0 = 10^{-5}\ M_\odot\ \mathrm{yr}^{-1}$.

cannot be neglected. The blend causes the profile of the 4957 Å feature to appear only slightly doubled, even in the absence of any wind (Fig. 5).

Blending from weaker lines also causes additional problems. In Figure 6 we compare the disk model with no wind, $i = 0°$, with SAO 22740, which has a spectral type (G2 Ib) similar to the mean disk spectral type at 5000 Å. Figure 6 shows the presence of the Ti I 5958.26 Å line in the red wing of the feature; this line is very strongly dependent on the effective temperature. The unidentified feature at 4959.20 Å is quite strong in the supergiant and should affect the wing of the 4957 Å line feature in FU Ori with the appropriate rotational velocity, but it cannot be inserted into the model spectrum in any reasonable way. (The equivalent width of this unidentified feature also increases substantially with decreasing effective temperature, much in the way that the Ti I 4958.26 Å line does.) Other features are probably present on the blue side of the 4957 Å line for which we have no identifications.

Our final model for the 4957 Å feature, shown in Figure 5 for a mass-loss rate of $1 \times 10^{-5}\ M_\odot\ \mathrm{yr}^{-1}$, produces a line blend that is not doubled, as observed, but has a larger equivalent width than indicated by the data. We feel that the agreement between theory and observation is reasonable, given the difficulties of modeling the blended spectrum. In particular, if the model continuum were depressed by approximately 10% by weak line blanketing (cf. Fig. 6), the agreement between theory and observations would become much better.[3]

We emphasize that our model results for the 4957 Å feature are the product of several adjustable parameters, such as log *gf*-values, turbulent velocities, and blends with unidentified features, in addition to the basic model parameters $\dot{M}_0$ and Γ. Thus, our calculations for this region are not definitive. However, the models demonstrate that for plausible wind parameters, the shape of the 4957 Å feature can be affected by mass loss in such a way as to suppress the double-peaked structure, as observed.

To summarize, we find that for mass-loss rates consistent with models for the Hα and Na I resonance lines, the Li I 6706 Å line should be relatively unaffected by mass loss, and the Fe II 5018 Å line should be strongly affected by the wind, as observed. The model prediction of a modest effect on the Fe I 4957 Å line by the wind is reasonably consistent with observations, considering the difficulties in synthesizing the spectrum in this region.

[3] Note that Petrov & Herbig (1992) report the residual intensity of the Fe I feature to be approximately 60%, in better agreement with the model than the observations shown in Fig. 5. The source of the observational discrepancy is not known.

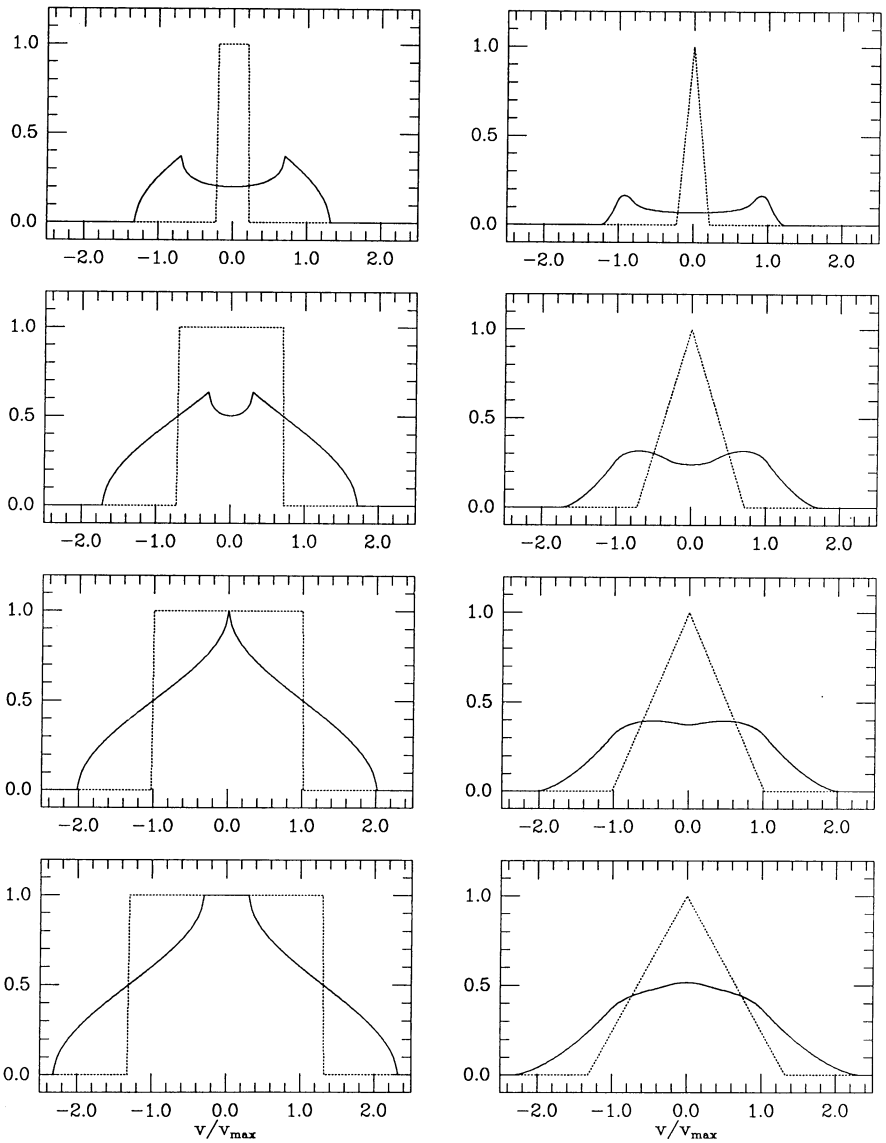

FIG. 4.—Schematic calculations showing the effects of convolution of disk rotational broadening with different intrinsic line shapes. The dotted lines show the assumed intrinsic line profile with no rotation, and the solid lines show the profile resulting from convolution with the disk annulus rotational profile Ψ (eq. [12]). The horizontal axis is measured in units of the disk rotation. The convolution of a triangular profile with disk rotation of comparable width (*right column of panels*) produces a profile with little or no indication of double-peaked structure. The convolution of a rectangular profile with disk rotation (*left-most panels*) can result in a sharply peaked profile if the intrinsic line width is comparable to the rotational velocity, which explains the origin of the sharp dip in the Fe II 5018 Å line profile (*bottom right panel in Fig. 3*).

3.4. *General Behavior of Line Profiles*

Petrov & Herbig (1992) studied the profiles of about 50 reasonably unblended (mostly neutral metallic) absorption lines in the blue spectrum of FU Ori. Many of these lines exhibited two absorption components. Petrov & Herbig showed that the velocity difference between the two absorption components decreases with decreasing residual line intensity (increasing line strength). In addition, Petrov & Herbig found that the long-wavelength absorption component becomes progressively blueshifted with increasing line strength, while the short-wavelength absorption component stays roughly at the same velocity (their Fig. 7).

The wind model qualitatively explains these effects. To show this without laboriously fitting every line blend, we constructed a sequence of line profiles for $\dot{M}_0 = 10^{-5}\ M_\odot\ \mathrm{yr}^{-1}$, using the wavelength and excitation parameters of the Fe I 4957.6 Å line, but using different *gf*-values. This should provide a qualitative treatment of the profiles of neutral metallic lines with excitation potentials $\sim$2.8 eV (typical of many lines in this spectral region).

In Figure 7 we display this sequence of Fe I profiles for differing *gf*-values. The velocity splitting between the two components decreases as the line strength increases. In addition, the blue absorption minimum remains at nearly the same velocity, ~ -40 to -35 km s^{-1}, while the red absorption minimum moves considerably closer to line center. Both of these effects are qualitatively similar to the results reported by Petrov & Herbig (1992). When the line is very strong, only one absorption minimum is observed, also in agreement with the results of Petrov & Herbig. It is difficult to make these com-

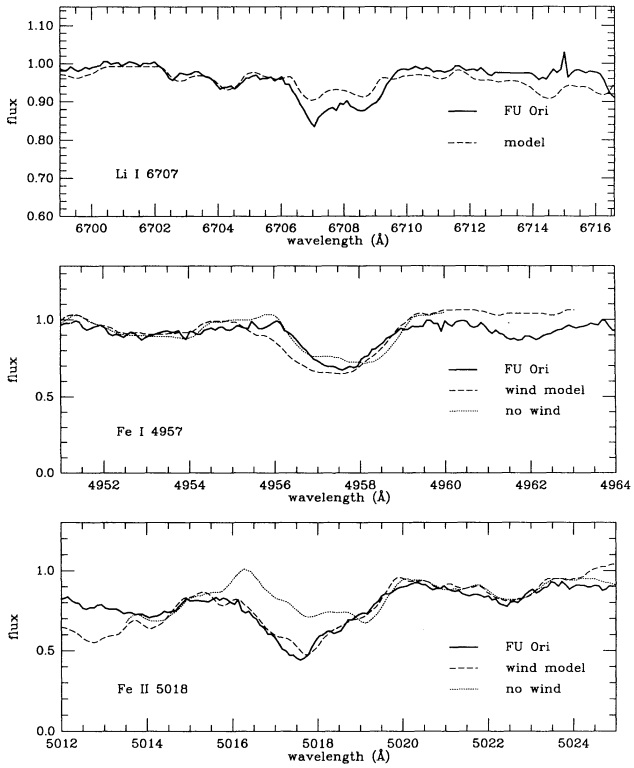

FIG. 5.—Line profiles of Fig. 4 summed over the entire disk, with $\dot{M}_0$ 1×10^{-5} $M_\odot$ yr^{-1} and $i = 35°$, compared with observations of FU Ori (*see text*).

parisons more quantitative, because small details of the line profiles depend sensitively on line blending, but it appears that the models reproduce the qualitative behavior of the observations.

3.5. *Near-Infrared CO Line Profiles*

Spectral observations at infrared wavelengths sample outer, cooler regions of the disk, compared with optical observations (KHH). Thus, mass-loss signatures in the infrared spectrum provide information on the variation of mass outflow with radius. Using cross-correlation analysis, Hartmann & Kenyon (1987a, b) and Kenyon & Hartmann (1989) suggested that the $v'' - v' = 2 - 0$ first-overtone absorption band of CO at 2.3 μm might be affected by mass loss. We applied the method of § 2 to calculate the 2.3 μm CO spectrum, using line parameters described in Calvet et al. (1991b). We consider the first-overtone $v'' - v' = 2 - 0$ and $v'' - v' = 3 - 1$ bands of CO. As shown in Figure 8, the spectrum synthesis produces band strengths in reasonable agreement with observation (see also Calvet et al. 1991a).

The introduction of a wind with $\dot{M}_0 \sim 10^{-5}$ $M_\odot$ yr^{-1} produces a small asymmetry in the $v'' - v' = 2 - 0$ band. The 4 m FTS spectrum of FU Ori is too noisy for individual lines to be compared with the model (Fig. 8). We therefore analyzed the average CO line profiles using cross-correlation analysis (cf. Hartmann & Kenyon 1987a, b; KHH). We used model calculations for no wind, $i = 0°$ as the template spectrum for both FU Ori and the wind model.

The cross-correlation results are shown in Figure 9. The model predicts a modest but significant asymmetry of the $v'' - v' = 2 - 0$ cross-correlation, indicating extra blueshifted

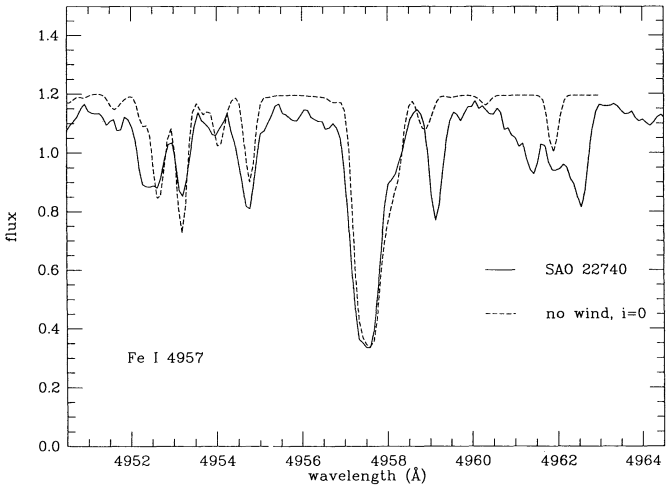

FIG. 6.—Comparison of the nonrotating ($i = 0$), no mass-loss disk model spectrum with the spectrum of a G2 supergiant of comparable effective temperature. We adopted a microturbulent velocity broadening of one-half the local sound speed and convolved the data with the 12 km s^{-1} FWHM instrumental profile. The line profile is significantly affected by a Ti I line at 4958.26 Å which is very sensitive to temperature. In addition, another unidentified but temperature-sensitive feature at 4959.2 Å affects the red wing of the line profile at the rotational velocity of FU Ori, but is not present in the model (*see text*).

absorption. This asymmetry is in reasonable agreement with the cross-correlation of the observed spectrum. The agreement with observations of the $v'' - v' = 2 - 0$ band may be slightly better for $\dot{M}_0 = 10^{-5}$ $M_\odot$ yr^{-1}, but it is not clear whether the limited signal-to-noise values of the observations can support such a distinction.

The cross-correlation of the $v'' - v' = 3 - 1$ region in FU Ori is almost perfectly symmetric; the model cross-correlations are only slightly asymmetric, with a larger asymmetry at higher mass-loss rates. As Kenyon & Hartmann (1989) suggested, the first excited vibrational state of CO has a lower population than the ground state in the cool wind, and so the wind is more transparent in the $v'' - v' = 3 - 1$ band.

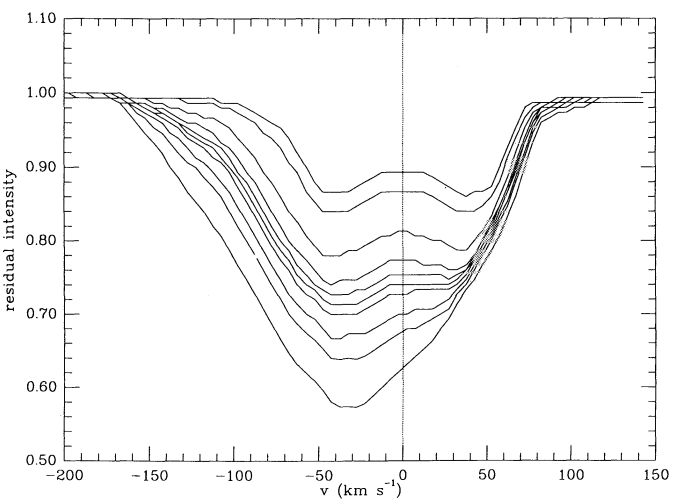

FIG. 7.—A sequence of disk model line profiles for $\dot{M}_0 = 10^{-5}$ $M_\odot$ yr^{-1}, for the wavelength and excitation parameters of the Fe I 4957.6 Å line, but a range of *gf*-values to illustrate the dependence of profile shape on line strength (*see text*).

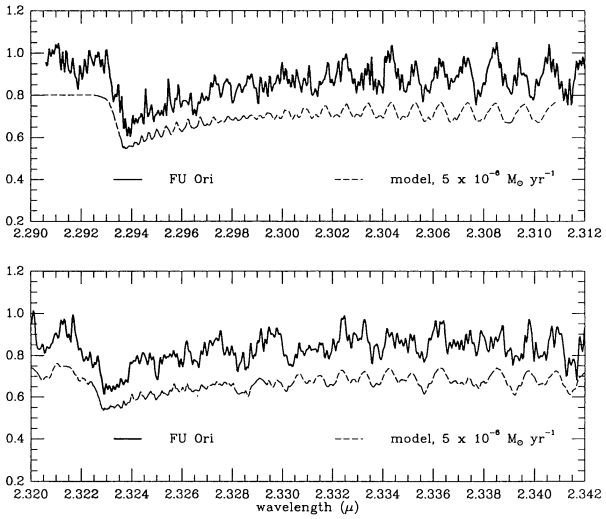

FIG. 8.—Model calculations of the $v'' - v' = 2 - 0$ (*upper panel*) and $v'' - v' = 3 - 1$ CO bands with $\dot{M}_0 = 5 \times 10^{-6}\ M_\odot\ \mathrm{yr}^{-1}$ compared with 4 m FTS observations of FU Ori (Hartmann & Kenyon 1987a). The model with $\dot{M}_0 = 1 \times 10^{-5}\ M_\odot\ \mathrm{yr}^{-1}$ is indistinguishable from the lower mass-loss rate model at this scale.

We find that mass-loss rates $\dot{M} \lesssim 10^{-6}\ M_\odot\ \mathrm{yr}^{-1}$ do not provide any measurable line asymmetry in the $v'' - v' = 2 - 0$ band. The reason for the discrepancy between our results and the estimate $\dot{M}_w \sim 10^{-7}\ M_\odot\ \mathrm{yr}^{-1}$ of Kenyon & Hartmann (1989) is that the latter failed to take the distribution of CO molecules over many rotational levels into account.

The model calculations for the near-infrared CO lines are consistent with the wind parameters $\dot{M}_0 = 5 \times 10^{-6}$–$1 \times 10^{-5}\ M_\odot\ \mathrm{yr}^{-1}$, $a_1 = 2$, $\Gamma = 1$, that is, roughly the same parameters as were used to fit the optical lines. However, it should be emphasized that the observational indications of mass loss in the CO first-overtone lines are marginal, and that we cannot rule out the possibility that the asymmetry of the $v'' - v' = 2 - 0$ band arises from absorption in a distant, cold, low-density circumstellar shell, rather than a disk wind (see discussion in Kenyon & Hartmann 1989). We also note that the CO results are somewhat dependent upon assumptions of dust formation (§ 3.1). These issues should be considered more carefully when higher signal-to-noise infrared spectra become available.

4. DISCUSSION

4.1. *Mass Loss, Line Profiles, and the Disk Hypothesis*

The results of § 3 show that relatively strong optical lines in the spectrum of FU Ori must show substantial departures from the simple double-peaked profiles produced by a rotating disk, assuming a wind of sufficient strength to explain the observed P Cygni Hα and Na I line profiles. Herbig (1989) and Petrov & Herbig (1992) called attention to the absence of double-peaked absorption-line profiles in the blue spectrum of FU Ori and argued that this fact poses a serious problem for the accretion disk hypothesis. Our results show that this is not the case, because a plausible disk wind model can reduce or eliminate line doubling. Moreover, we have shown that the very simple disk wind model considered here can reproduce the profiles of representative lines reasonably well. The disk wind model also explains the reduction in velocity spread between the absorption dips and the increasing blueshift of the

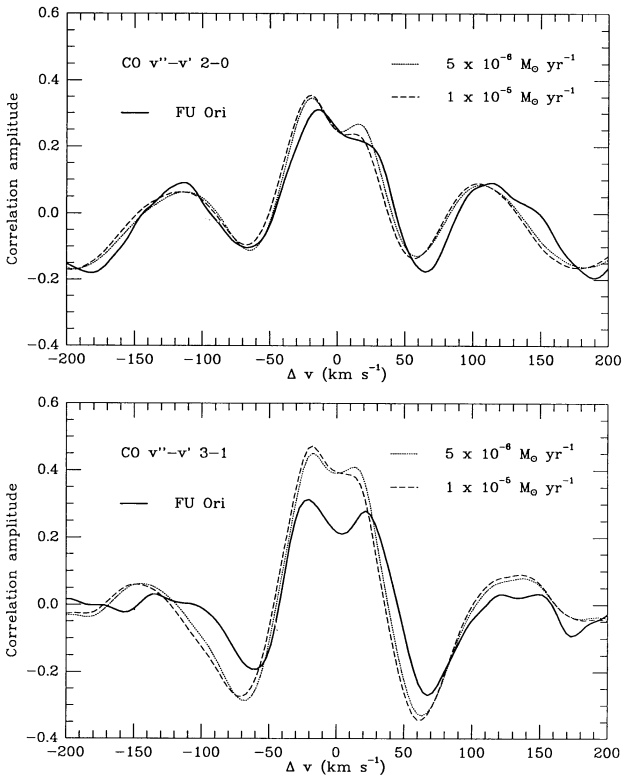

FIG. 9.—Cross-correlations of selected CO first-overtone band regions. The calculated model spectrum without wind and rotation was used as a template both for the wind models and for FU Ori. The top panel is the correlation of the spectral region between 2.291 and 2.310 μm, which includes much of the $v'' - v' = 2 - 0$ band away from the bandhead; the lower panel is the correlation of the region between 2.321 and 2.349 μm for the $v'' - v' = 3 - 1$ band.

long-wavelength absorption component with increasing line depth observed by Petrov & Herbig (1992) in many lines (cf. § 3.4).

4.2. *Disk Wind versus Stellar Wind*

The strongest argument for the disk wind model is its success in explaining the *differential* behavior of line profiles. However, one might consider whether a stellar wind model (Fig. 1), such as the model of Shu et al. (1988) specifically proposed for T Tauri stars, might also explain the observations. We cannot draw firm conclusions in the absence of detailed calculations of the stellar wind velocity field as a function of position, but some general considerations are suggested.

The biggest problem for the stellar wind model is the requirement of small blueshifts in lines of intermediate strength. The problem arises because the optical continuum light comes from an extended region of the disk, of area comparable to or larger than the star. In typical wind models, the expansion velocity increases to a value comparable to the escape velocity over a distance of a few stellar radii, roughly the same size as the optical continuum emission region of the disk (cf. Fig. 1). Therefore the stellar wind seen in projection over most of the disk should exhibit relatively high velocities $\sim 100\ \mathrm{km\ s}^{-1}$. The wind will have velocities of a few tens of km s^{-1} only in a small region near the star, and this region would be projected against such a small fraction of the inner disk that it could not contribute much to the total spectrum. Thus, it is difficult to reproduce the small blueshifts seen in lines of inter-

mediate strength with a model in which the wind comes from the star, but the background continuum emission comes from an extended disk. (If the background continuum does not come from a disk, it is difficult to understand the ubiquitous double-peaked profiles of weak lines; cf. Welty et al. 1992.)

Rotational velocities also pose a problem for a stellar wind model. In the Shu et al. (1988) theory, the cold wind is driven by stellar rotation close to breakup velocity. In our model, with a central star of mass 0.49 $M_\odot$ and radius 4.42 $R_\odot$, the breakup velocity of the central star is ~ 150 km s^{-1}. If the magnetic field lines enforce corotation out to only $\sim 2R_i$ (cf. Shu et al. 1988), the rotational velocity of the wind could approach ~ 300 km s^{-1}. Such a large rotational broadening is inconsistent with the observed widths of many lines (cf. Fig. 5) unless all FU Ori objects are viewed nearly pole-on.

The problems for a stellar wind model become very difficult if the blueshifted $v'' - v' = 2 - 0$ CO absorption is confirmed and is shown to arise in an accelerating wind rather than in a distant circumstellar shell. It is hard to imagine that a stellar wind of several hundred km s^{-1} could flow out to $\sim 10R_i$, where the 2 μm continuum is formed, with a projected velocity shift of only ~ 20–30 km s^{-1} (Fig. 9). The asymmetries of the CO lines should be explored in more detail with much higher signal-to-noise spectra now obtainable with infrared array spectrometers.

4.3. *Wind Rotation*

The observed Fe II line profile in Figure 5 shows an absorption "dip" of the type naturally interpreted as a "shell" of material at nearly constant velocity (e.g., Herbig 1966). However, the rotating wind model is able to reproduce this "dip" without exhibiting any true "shell" in expansion velocity. Instead, as shown in Figure 3, the wind is uniformly accelerating, and produces an intrinsically square line profile. The "dip" arises *because the wind is rotating.* We suggest that many "shell" lines of FU Ori arise in a rotating, differentially expanding wind.

As shown in Figures 3 and 4, the "shell" feature appears only when the projected rotational velocity of the wind is comparable to the intrinsic absorption-line width. In our wind model with cylindrical rotation, this means that the dip will only appear at velocity shifts ~ 40–60 km s^{-1}. FU Orionis objects also show evidence for very high velocity shells (Herbig 1966, 1977; Bastian & Mundt 1985), which are unlikely to be explained by wind rotation effects.

4.4. *Disk Wind Properties*

Croswell et al. (1987) showed that the low-temperature wind of FU Ori cannot be driven by thermal pressure, and there is no obvious source of radiation pressure to provide the required acceleration. Thus, the most attractive mechanism for driving the flow is acceleration by rotating magnetic field lines, as in the extragalactic jet model of Blandford & Payne (1982) and the pre–main-sequence disk wind models of Pudritz & Norman (1983) and Königl (1989). In this context, the significance of interpreting the blueshifted "shell" features as arising in a rapidly rotating wind is obvious.

In the self-similar Blandford & Payne (1982) model, $\dot{M}_w(r) \propto \ln(r)$; Pudritz & Norman (1983) and Königl (1989) employed this scaling to construct steady disk models in which the wind carries off all angular momentum required for steady disk accretion. However, this can only be achieved for a very specific magnetic field configuration in the disk, and theory cannot at present predict disk magnetic fields with any confidence. The actual behavior of pre–main-sequence disk winds must be constrained observationally.

Our results suggest that the outflow of FU Ori originates over a substantial area of the inner accretion disk, but not over many decades in radius as suggested by the original Pudritz & Norman and Königl models. As discussed in § 3.1, if dust is not destroyed at temperatures cooler than $\lesssim 10^3$ K, a massive wind produces unacceptably large extinction and infrared excess. This implies that the mass-loss rate falls off faster with radius than in the self-similar model beyond about $12R_i$. If the blue-shifted absorption in the $v'' - v' = 2 - 0$ CO lines arises in a distant circumstellar shell rather than a wind, significant mass loss is limited to a region of several R_i near the central star.

Recently Pelletier & Pudritz (1992) have argued that a nonself-similar scaling is most appropriate for magnetized accretion disk winds and suggest that there might be an "outer edge" to the wind. For their fiducial parameters, the outer edge is at $\sim 17R_i$, roughly where we truncated our wind models. It is possible that the wind limit found by Pelletier & Pudritz is sufficient to avoid large dust optical depths in the wind from the outer disk.

Estimates of mass-loss rates depend upon the choice of velocity gradient. We have not been able to reproduce the FU Ori observations with velocity gradients $\Gamma \sim$ unity for $\dot{M}_0 = 10^{-6}\ M_\odot$ yr^{-1}. Conversely, the mass loss from the optical region of the disk cannot be as large as $10^{-4}\ M_\odot$ yr^{-1}, because then the wind would be optically thick in the continuum. In this case *all* of the absorption lines would be blue-shifted by tens of km s^{-1}, whereas the FU Ori objects are all within a few km s^{-1} of the neighboring interstellar medium (Herbig 1966, 1977; Hartmann & Kenyon 1987a, b). Thus, our results reinforce the estimate of $\dot{M}_w \sim 10^{-5}\ M_\odot$ yr^{-1} found by Croswell et al. (1987) from a study of the Hα and Na I line profiles.

The ratio of the kinetic energy loss in the wind L_w to the accretion energy is

$$L_w/L_{\rm acc} = (\dot{M}_w V_w^2/2L_{\rm acc})\ . \tag{14}$$

Our estimates of $\dot{M}_w \sim 10^{-5}\ M_\odot$ yr^{-1} and a terminal wind velocity $V_w \sim 300$ km s^{-1} imply $L_w \sim 0.3L_{\rm acc}$. This result is an order of magnitude estimate, but it does suggest that the wind may be an important component of the energy budget of the inner disk.

The ratio of wind angular momentum loss to the angular momentum transfer required for steady accretion at $\dot{M}_{\rm acc}$ is more difficult to estimate. Averaged over the inner disk, this ratio is

$$\dot{J}_w/\dot{J}_{\rm acc} \sim (\dot{M}_w/\dot{M}_{\rm acc})(\Omega r_{\rm A}^2/\Omega_{\rm K} r^2)\ , \tag{15}$$

where $r_{\rm A}$ is the Alfvén radius of the wind and $\Omega_{\rm K}$ is an average Keplerian angular velocity in the inner disk. If we take $\Omega r_{\rm A} \sim V_w$ and $\Omega \sim \Omega_{\rm K}$ (Pudritz & Norman 1986), $\dot{M}_w \sim 10^{-1}\ \dot{M}_{\rm acc}$, and $\Omega_{\rm K} r \sim 100$ km s^{-1}; the results suggest that the wind may carry away an appreciable fraction of the inner disk angular momentum. However, the limits on mass loss at large radii discussed above indicate that the wind is very unlikely to carry away most of the angular momentum from the *outer* disk.

4.5. *Boundary Layer Visibility*

If the self-similar scaling holds to the smallest radii, we find that the wind from the innermost disk regions is optically thick in the continuum (§ 3). This material would help to absorb or

"hide" any "boundary layer" emission from the inner edge of the disk. In simple disk models, the boundary layer is the narrow disk region where material in Keplerian rotation loses enough energy to come to rest on the slowly rotating star (Lynden-Bell & Pringle 1974). It is interesting to speculate whether the absorption of boundary layer emission in a optically thick wind over an area $\sim R_i^2$ could account for the nondetection of boundary layer radiation from FU Ori objects (Kenyon et al. 1989).

4.6. *Collimation of the Wind*

We have assumed that the disk wind of FU Ori is perfectly collimated, that is, the expansion velocity is only along the z-(rotation) axis. In the disk wind models of Blandford & Payne (1982), Pudritz & Norman (1983), and Königl (1989), the cold, centrifugally driven winds are efficiently accelerated only when the field lines near the disk are bent away from the z-direction by more than 30°. This implies that the flow must have an expansion velocity in r as well as in z.

It is straightforward to show that a rotating ring, expanding with a velocity v_w making an angle θ_w with the z-axis, has a line profile with the same form as equation (12), but with $V_{\max}$ increased by a factor of $(1 + v_w^2 \sin^2 \theta_w / V_{\rm Kep}^2)^{1/2}$. If $\theta_w \sim 30°$, the line profile width of an individual ring is not greatly affected unless $v_z \gtrsim V_{\rm Kep}$. However, an absorption line that is optically thick out to such a large velocity will exhibit a line width that is dominated by expansion anyway, since the observed line profile is an integration over rings at different (z) levels with different expansion velocities. For this reason, and to avoid introducing another free parameter, our neglect of the r-component of the velocity seems justified in this initial disk wind treatment. Models with more complicated geometries may be able to constrain the collimation of the wind as it leaves the disk surface.

5. SUMMARY

The disk wind model provides a natural explanation of the peculiar line profiles of FU Ori. Using the same mass-loss rate estimated by Croswell et al. (1987) from an analysis of the Hα and Na I line profiles, we find that we can approximately reproduce profiles of representative lines with different absorption strengths. Most important, the model predicts *differential* line profile shifts and changes in shape. This differential behavior results from the acceleration of the wind through the outer disk photosphere, which *must* occur in a continuous disk wind. The general predictions of profiles from a continuous wind model are in qualitative agreement with observed trends. It appears to be difficult for typical stellar wind models to reproduce the small velocity shifts observed in lines of intermediate strength. Our results support the picture in which the massive wind of FU Orionis emanates from the surface of a rapidly accreting pre–main-sequence disk.

We are indebted to Rob Hewett for help with data reduction and analysis and to R. Kurucz for kindly providing his list of spectral lines. We also acknowledge useful comments by Ralph Pudritz. This research was supported in part by NASA grant NAGW-511 and by the International Exchange Program of the Smithsonian Institution.

REFERENCES

Adams, F. C., Lada, C. J., & Shu, F. H. 1987, ApJ, 312, 788
Basri, G., & Bertout, C. 1989, ApJ, 341, 340
Bastian, U., & Mundt, R. 1985, A&A, 144, 57
Bertout, C., Basri, G., & Bouvier, J. 1988, ApJ, 330, 350
Blandford, R. D., & Payne, D. G. 1982, MNRAS, 199, 883
Calvet, N., Hartmann, L., & Kenyon, S. J. 1991a, ApJ, 383, 752
Calvet, N., Patiño, A., Magris, C. G., & D'Alessio, P. 1991b, ApJ, 380, 617
Clarke, C. J., Lin, D. N. C., & Pringle, J. E. 1990, MNRAS, 242, 439
Croswell, K., Hartmann, L., & Avrett, E. H. 1987, ApJ, 312, 227
Edwards, S., Ray, T. P., & Mundt, R. 1992, in Protostars and Planets III, ed. E. H. Levy & M. S. Mathews, in press
Hartigan, P., Hartmann, L., Kenyon, S., Hewett, R., & Stauffer, J. 1989, ApJS, 70, 899
Hartmann, L., & Kenyon, S. J. 1985, ApJ, 299, 462
———. 1987a, ApJ, 312, 243
———. 1987b, ApJ, 322, 393
———. 1991, in IAU Colloq. 129, Structure and Emission Properties of Accretion Disks, ed. C. Bertout, S. Collin-Souffrin, J. P. Lasota, & J. Tran Thanh Van (Paris: Éditions Frontières), 203
Hartmann, L., Kenyon, S. J., & Hartigan, P. 1992, in Protostars and Planets III, ed. E. H. Levy & M. S. Mathews, in press
Hartmann, L., & MacGregor, K. B. 1982, ApJ, 259, 180
Hartmann, L., & Stauffer, J. R. 1989, AJ, 97, 873
Herbig, G. H. 1966, Vistas Astron., 8, 109
———. 1977, ApJ, 217, 693
———. 1989, in ESO Workshop on Low Mass Star Formation and Pre–Main-Sequence Objects, ed. B. Reipurth (Garching: ESO), 233
Kenyon, S. J., & Hartmann, L. 1987, ApJ, 323, 714
———. 1989, ApJ, 342, 1134
Kenyon, S. J., Hartmann, L. W., & Hewett, R. 1988, ApJ, 325, 231 (KHH)
Kenyon, S. J., Hartmann, L., Imhoff, C. L., & Cassatella, A. 1989, ApJ, 344, 925
Königl, A. 1989, ApJ, 342, 208
Lada, C. J. 1985, ARA&A, 23, 267
Lovelace, R. V. E., Wang, J. C. L., & Sulkanen, M. E. 1987, ApJ, 315, 504
Lynden-Bell, D., & Pringle, J. E. 1974, MNRAS, 168, 603
Pelletier, G., & Pudritz, R. E. 1992, ApJ, 394, 117
Petrov, P. P., & Herbig, G. H. 1992, ApJ, 392, 209
Pringle, J. E. 1989, MNRAS, 236, 107
Pudritz, R. E., & Norman, C. A. 1983, ApJ, 274, 677
———. 1986, ApJ, 301, 571
Reipurth, B. 1989, Nature, 340, 42
———. 1990, in IAU Symp. 137, Flare Stars in Star Clusters, Associations, and the Solar Vicinity, ed. L. V. Mirzoyan, B. R. Petterson, & M. K. Tsvetkov (Dordrecht: Reidel), 229
Ruden, S. P., Glassgold, A. E., & Shu, F. H. 1990, ApJ, 361, 546
Shakura, N. I., & Sunyaev, R. A. 1973, A&A, 24, 337
Shu, F. H., Lizano, S., & Adams, F. C. 1987, ARA&A, 25, 23
Shu, F. H., Lizano, S., Ruden, S. P., & Najita, J. 1988, ApJ, 328, L19
Steenbock, W., & Holweger, H. 1984, A&A, 130, 319
Terebey, S., Vogel, S. N., & Myers, P. C. 1989, ApJ, 340, 472
Welty, A. D., Strom, S. E., Edwards, S., Kenyon, S. J., & Hartmann, L. W. 1992, ApJ, 397, 260